PAPER Nr. : 16

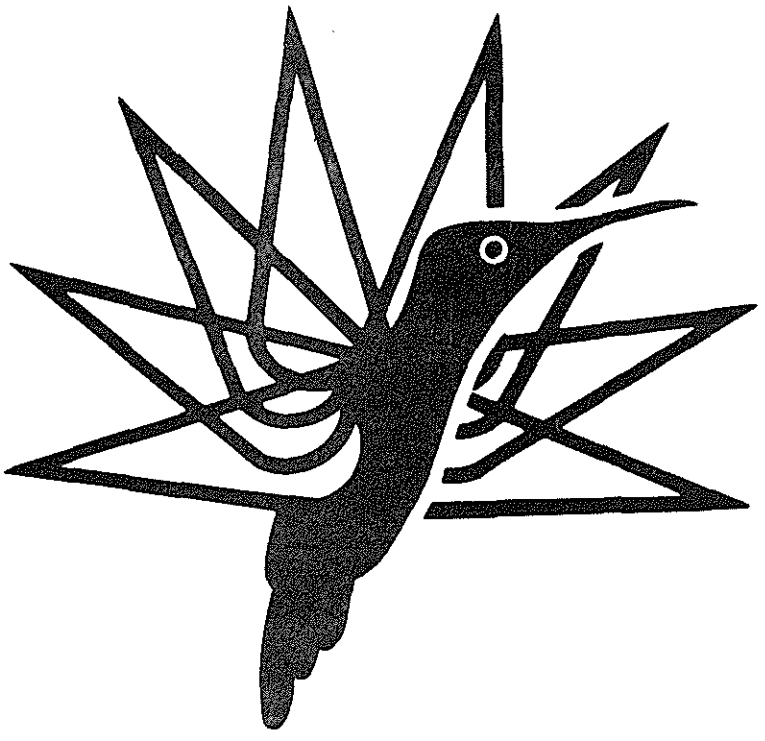

THEORETICAL STUDY OF TWO DIMENSIONAL STALL IN AN INCOMPRESSIBLE FLOW

by

J.J. COSTES
Office National d'Etudes et de Recherches Aérospatiales
BP 72 - 92322 Châtillon Cedex, FRANCE

TENTH EUROPEAN ROTORCRAFT FORUM

AUGUST 28 – 31, 1984 – THE HAGUE, THE NETHERLANDS

Abstract

This paper presents, for an incompressible fluid, a simplified method to predict aerodynamic forces on a stalled airfoil. In the circulating flow region, the pressure remains approximatively constant. This experimental fact allows the use of potentials to model the flow field. Computations are presented, first in the steady case, with comparisons to the experimental lift, moment, and drag forces, and an extension has been attempted for the oscillating airfoil.

1. Introduction

One of the most important problems concerning the aerodynamics of the helicopter rotor is the unsteady stall occuring on the retreating blade. This subject has been extensively studied by numerous authors. Their work may be sorted in two classes. The first one is an attempt to mathematically modelise the aerodynamic forces without much regard to the actual flow 3 , 4 , 5 . In the second class, the Navier-Stokes equations are solved but the expense in computation time is too large for an extensive use in the industry.

In 1978 two authors, Maskew and Dvorak have presented a paper 1 where a simplified flow modelisation was described. One will found in the present paper the same basic assumption though different singularities, namely sources and doublets, are used to compute the potentials. The method has also been extended to the case of an airfoil executing small unsteady oscillations in pitch around a preselected mean incidence.

2. Assumptions and fundamental equations

2.1. Conservation of the mass and momentum

The fluid is supposed to be incompressible without viscosity. The velocity may be expressed as the gradient of a scalar potential φ in motionless axes of reference.

$$V = \operatorname{grad} \varphi$$

The conservation of the mass theorem gives :

(1) $$\frac{\partial^2 \varphi}{\partial x^2} + \frac{\partial^2 \varphi}{\partial y^2} = 0$$

The conservation of momentum links the acceleration $\vec{\gamma}$ of the fluid to the pressure gradient by :

(2) $$\rho \vec{\gamma} + \overrightarrow{\operatorname{grad} p} = 0$$

ρ being the density of the fluid.

No linearisation hypothesis is necessary to obtain (1) and (2).

2.2. Green's formula

Application of Green's formula to a domain D, with a border Γ, leads to expression (3).

(3) $$-\frac{1}{2\pi} \int_\Gamma \left[\operatorname{Log} r \frac{\partial \varphi}{\partial n} - \varphi \frac{\partial}{\partial n} \operatorname{Log} r \right] ds = \begin{cases} \varphi(P) \text{ if } P \text{ is inside } \mathcal{D} \\ 0 \text{ if } P \text{ is outside } \mathcal{D} \end{cases}$$

$-\frac{1}{2\pi} \operatorname{Log} r$ is the source kernel in 2.D

$-\frac{1}{2\pi} \frac{\partial}{\partial n} \operatorname{Log} r$ is the doublet kernel in 2.D.

n is the normal to the border Γ directed towards the interior of D.

The potential φ and its derivatives are supposed to satisfy continuity conditions on D as well as on border Γ. Relation (3) may not be directly applied because the probleme of interest is the determination of the flow around an obstacle. Nevertheless, by considering a circle of radius R, of center C inside D, which may become as large as desired ; application of relation (3) to the exterior of D gives (4) when the perturbations at infinity be may neglected.

$$(4) \qquad \varphi(P) = -\frac{1}{2\pi}\int_{\Gamma}\left[\mathcal{L}og\, r\,\frac{\partial\varphi}{\partial n} - \varphi\,\frac{\partial}{\partial n}\mathcal{L}og\, r\right] ds$$

Continuity of φ and its derivatives outside of D is assumed. A circulation around D is not allowed without correction of (4) to take into account the perturbation at infinity.

3. Flow field around a cylinder with a circular basis

3.1. Discretisation of the problem

Let us consider an obstacle D of circular shape in translation within a fluid, with velocity U_∞ directed along axis X. The flow velocity is $V = -U_\infty \vec{\imath} + \overrightarrow{grad}\,\varphi$

$\vec{\imath}$; vector of length 1 in the direction of the X axis.

The non-separation condition along border Γ gives the value of $\frac{\partial\varphi}{\partial n}$:

$$(5) \qquad \frac{\partial\varphi}{\partial n} = U_\infty \sin\theta$$

the tangent to Γ makes angle θ with axis X.

Since $\frac{\partial\varphi}{\partial n}$ is known, relation 4 allows the computation of φ on every point P outside of D , as soon as φ is determined on border Γ. This is done by approximating Γ by a polygon, on each side of the polygon sources and doublets with constant intensities are placed. The intensities of the sources is given by (5). The intensities of the doublets is unknown, but is determined by the expression of (4) on the middle of each segment, thus providing a linear set of equations, the solution of which giving an approximation of φ on Γ.

Remark : the use of a linear variation of the doublets intensities on the polygon segments does not give a better solution.
At least for a polygon with an even number of equal length sides, the linear system is undetermined. The mathematical solution is not unique, the difference between two solutions is a non physically acceptable flow field.

3.2. Elementary flow fields

a) The potential created at $P(x_0, y_0)$ by a segment of sources with constant intensities is given by :

$$\varphi(P) = -\frac{1}{2\pi}\int_{x_1}^{x_2} \mathcal{L}og\, r\, dx$$

This relation may be integrated by making use of the elementary functions, the derivation of φ gives the velocity of the flow.

b) The potential created at $P(x_0, y_0)$ by a segment of doublets with intensity $Q(x)$ is given by :

$$\varphi(P) = -\frac{1}{2\pi}\int_{x_1}^{x_2} \frac{Q(x)\, y_0\, dx}{(x-x_0)^2 + y_0^2}$$

The segment is supported by the x axis and bounded by x_1, and x_2 Streamlines for an intensity by unit length $Q(x)$ constant are given in figure 1. When the intensity varies linearly between - 1 and + 1, the flow is given in figure 2. The jump in the tangential component of the velocity across the segment is to be noticed. A linear variation of the doublets intensity can be used to modelise the lines of vorticies.

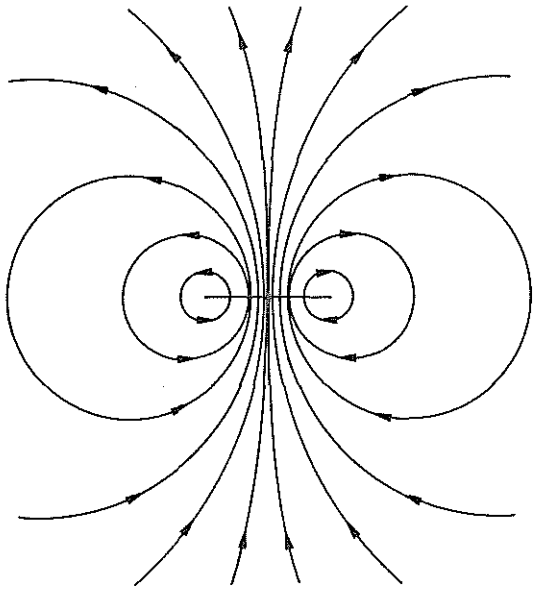

Fig. 1 — Streamlines induced by a segment supporting doublets of constant intensity by unit length.

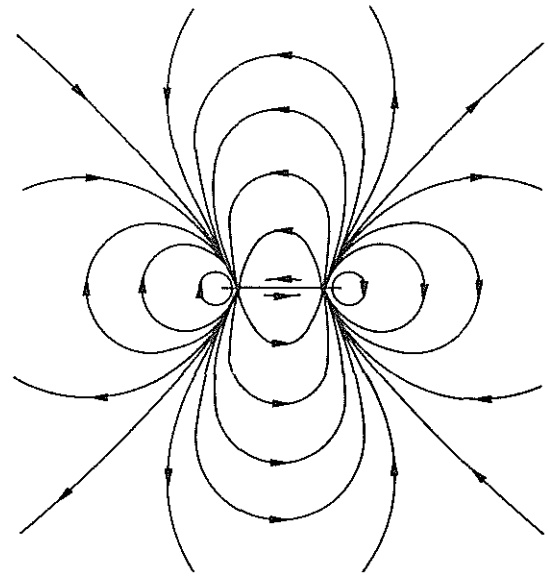

Fig. 2 — Streamlines induced by a segment of doublets whose intensity varies linearly between $Q = -1$ and $Q = +1$.

3.3. Example of computation, flow fields without circulation

Using the process described in the preceding paragraph, the flow field around a cylinder with a circular basis is computed. The value of the potential on the middle of each side of the polygon is obtained. The next step is to calculate the pressure, the Bernouilli's relation may be used :

$$(6) \qquad p + \frac{1}{2}\rho V^2 = p_\infty + \frac{1}{2}\rho U_\infty^2$$

By making use of the C_p coefficient, relation 6 is transformed in :

$$(7) \qquad C_p = \frac{p - p_\infty}{\frac{1}{2}\rho U_\infty^2} = 1 - \left(\frac{V}{U_\infty}\right)^2$$

The total velocity V is composed of two parts, the first is the velocity at infinity U_∞ and the second part is the velocity induced by the sources and doublets placed on the polygon sides. On the obstacle boundary, the computation of V is particularly simple. The potential is determined on the polygon sides, and thus the tangential component $\frac{\partial \varphi}{\partial s}$ is known. The normal component is given by relation (5). If θ is the angle between the local tangent to the obstacle and the x axis, the total velocity V is :

$$V = \frac{\partial \varphi}{\partial s} - U_\infty \cos\theta$$

When the circle is approximated by a regular polygon with a sufficient number of sides (at least 28), the agreement with the theory is excellent concerning the C_p on the circle.

3.4. Flow field with circulation

A circulation may be desired around the cylinder circular basis, but this circulation cannot be taken into account by the potential φ because of the conditions of validity on relation (4). The circulation is then artificially introduced in the complementary flow, in the same way as the uniform velocity U_∞ of the preceding paragraph has been introduced. The simplest possibiliby is to put a concentrated vortex at the center of the circle, the vortex intensity is adjusted to obtain a stagnation point at a preselected position on the circle. Numerical results are in excellent agreement with the theory. Nevertheless, there is no reason to impose the vortex position at the circle center. When the vortex is displaced towards the circle perimeter, the numerical results are worsening gradually. They may be improved by an augmentation of the number of polygon sides, but this is only an expedient. The cause of the degradation is evident ; the non-separation condition is enforced only on the middle of each side of the polygon. By doing this, one supposes that the variations of the fluid velocity are small on the polygon sides. One must then avoid the presence of a concentrated singularity such than a vortex close to the polygon border. Keeping in mind a possible extension to actual profiles, a possibility is the use of a repartition of vorticies with constant strength all over the obstacle border. In the particular case of a circle, it may be proved that the induced velocities are the same as those created by a concentrated vortex at the circle center.

4. Flow field around a profile without separation

4.1. Steady problem

By comparison to the problem of the flow around a circle with circulation, an additional difficulty is introduced by the acute angle at the trailing edge. When constant strength vorticies are placed on the profile perimeter, they introduce large variations of velocity at the trailing edge. This unfavourable situation may be alleviated by making the vortex strength to decrease towards zero at the trailing edge on the upper surface as well as on the lower surface. The simplest possibility is the use of a parabolic shape for the variation of the intensity of the vorticies along the profile surface. One remains with only one adjustable coefficient, the maximum value of the intensity, reached towards the leading edge when the curvilinear abscissa on the profile perimeter is at is mean value. In order to simplify the mathematical derivations, the intensity of the vorticies varies linearly on the polygon sides while approximating the prescribed parabolic shape.

A comparison with the theory has been attempted in the case of a family of symmetrical Joukowski's profiles with various thickness.
The profiles are obtained by the following operations :

- A circle is first defined by the relations :

$$X = -b + (a+b)\cos\theta$$
$$Y = (a+b)\sin\theta \qquad 0 \leq \theta \leq 2\pi$$

- The profile is then obtained by a transformation of the circle :

$$x = X + \frac{a^2 X^2}{X^2+Y^2} + \frac{2b^2}{a^2+2b}$$

$$y = Y - \frac{a^2 Y}{X^2+Y^2}$$

If $\lambda = \frac{b}{a}$, and the parameter a is chosen such that $a = \frac{1+2\lambda}{2(1+\lambda)^2}$ the chord of the profile is equal to 2. The flow field around the profile is determined by the transformation of the flow field around the circle. If the angle of incidence of the profile is α, the lift coefficient C_L is given by :

$$C_L = 2\pi \frac{(1+2\lambda)}{1+\lambda} \sin\alpha$$

For small angles of incidence, the variation of C_L with the incidence is equal to :

$$\frac{dC_L}{d\alpha} = 2\pi \frac{(1+2\lambda)}{1+\lambda}$$

On figure 3, a comparison between the computed $\frac{dC_L}{d\alpha}$ and the theoretical value is given. With 28 sides for the definition of the profile, the agreement is perfect down to a thickness ratio of 6 %. An augmentation of the number of sides improves the numerical results, which remain good down to 4 % with 34 sides.

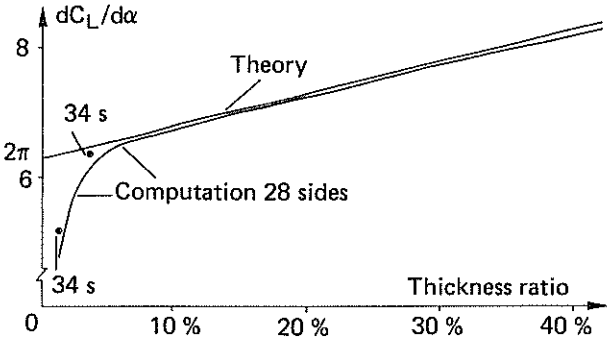

Fig. 3 – The profile is approximated by a polygon with 28 sides and the computed value of $dC_L/d\alpha$ is compared with the theory. When the number of sides is increased, the results are improved for low thickness ratios. Two results are presented with 34 sides.

4.2. Unsteady problem

a) Derivation of the fundamental equations :

The profile is supposed to undergo small displacements around a given mean position. In an absolute set of axes, the velocity V is given by :

$$V(X,Y,t) = V_0(X,Y,t) + v(X,Y,t)$$

V_0 is the flow velocity computed in the steady case, it is not dependent of time in a set of axes in translation with the profile. The term v is induced by the profile oscillations and is infinitely small (order 1).

The equations of conservation for the fluid mass and momentum will be linearised to order 1. The equation of continuity is :

$$div(V) = div(V_0) + div(v) = 0$$

V_0 being the solution of the steady case $div(V_0)=0$. One may then conclude :

(8) $$div(v)=0$$

The velocities v and V_0 are supposed to derive from the potentials φ and Φ_0 expressed in the absolute axes.
Relation (8) becomes :

(9) $$\Delta\varphi = \frac{\partial^2\varphi}{\partial x^2} + \frac{\partial^2\varphi}{\partial y^2} = 0$$

Because of (9), Green's formula may also be applied to the unsteady potential . The equation of conservation for the fluid momentum is :

(10) $$\rho\vec{\Gamma} + \overrightarrow{grad}\, P = 0$$

where $\vec{\Gamma} = \vec{\Gamma_0} + \vec{\gamma}$ and $P = P_0 + p$.

The $\vec{\Gamma_0}$ and P_0 are the acceleration and pressure steady parts and the $\vec{\gamma}$ and p are the acceleration and pressure created by the profile oscillations. The acceleration Γ is obtained by the total derivative of V, that is to say a derivation of along a fluid particle path :

$$\vec{\Gamma} = \frac{d}{dt}(\vec{V}) = \frac{d}{dt}(\vec{V_0} + \vec{v})$$

The component Γ_i may be written as :

(11) $$\Gamma_i = \frac{\partial}{\partial t}(V_{oi} + v_i) + (V_{oj} + v_j)(V_{oi} + v_i)_{,j}$$

By neglecting the terms of order 2, the equation 11 becomes :

(12) $$\Gamma_i = \Gamma_{oi} + \frac{\partial v_i}{\partial t} + v_j V_{oi,j} + V_{oj} v_{i,j}$$

Replacing Γ by its value, relation (10) gives :

(13) $$\rho\left[\Gamma_{oi} + \frac{\partial v_i}{\partial t} + v_j V_{oj,j} + V_{oj} v_{i,j}\right] + P_{o,i} + p,i = 0$$

P_0 and Γ_0 are solutions for the steady problem then :

$$\rho\Gamma_{oi} + P_{o,i} = 0$$

Using the potentials φ and Φ_0 equation (13) is finally transformed in :

(14) $$-p,i = \rho\left[\frac{\partial\varphi_i}{\partial t} + (\varphi_{,j}\Phi_{0,j})_{,i}\right]$$

this equation may be integrated on the geometrical variables, which gives :

(15) $$-p = \rho\left[\frac{\partial\varphi}{\partial t} + (\varphi_{,j}\Phi_{0,j})\right] + p_0(t)$$

The constant of integration p_0 may depend on time. In the case of an unstalled profile, this constant is equal to zero, because the potentials φ and Φ_0 as well as the pressure p are supposed to be zero at infinity.

It is often more convenient to express the potentials Φ_0 and φ, as well as their derivatives in a set of axes translating with the profile at the constant velocity U_∞.

$\Phi_0(X,Y,t) \equiv \tilde{\Phi}(x,y)$ ($\tilde{\Phi}$ does not depend on time t)

$$\varphi(X,Y,t) \equiv \tilde{\varphi}(x,y,t)$$

relation (15) is now transformed in :

$$(16) \qquad -p = \rho \left[\frac{\partial \tilde{\varphi}}{\partial t} + U_\infty \frac{\partial \tilde{\varphi}}{\partial x} + \tilde{\varphi}_{,j} \tilde{\Phi}_{,j} \right]$$

b) unsteady wake

Alternate vorticies are shed by the trailing edge, they are carried by the steady flow with velocity $V_o(x,y)$. The vorticies mean path is the streamline originating from the trailing edge. A jump of potential is allowed across this streamline but there is no jump of pressure. This condition gives :

$$(17) \qquad \frac{\partial \varphi^+}{\partial t} + \varphi^+_{,j} \Phi^+_{o,j} = \frac{\partial \varphi^-}{\partial t} + \varphi^-_{,j} \Phi^-_{o,j}$$

The signes + and - are referring respectively to the flow above and below the vorticies path. For the steady flow field, there is no jump of velocity across the wake ; $\Phi^+_{oj} = \Phi^-_{oj} = V_{oj}$

Relation (17) may be rewritten as :

$$(18) \qquad \frac{d}{dt} \left[\varphi^+ - \varphi^- \right] = \frac{\partial}{\partial t} \left[\varphi^+ - \varphi^- \right] + \vec{V_o} \, \overrightarrow{grad} \left[\varphi^+ - \varphi^- \right] = 0$$

The total derivative of the potential jump $\varphi^+ - \varphi^-$ is equal to zero. This simply means that the jump of potential is carried along the streamline with the local velocity V_o of the steady flow field.

c) Discretisation of the unsteady problem

The profile is approximated by a 50 sided polygon, its vibration is harmonic, thus the unsteady potential $\tilde{\varphi}$ is also harmonic and may be defined by a complex number multiplied by $Exp(j\omega t)$. On each side of the polygon are placed unsteady sources and doublets the intensities of which are constant complex numbers on the side length. The sources intensities are determined by unsteady non-separation conditions obtained by linearisation of the general non-separation condition.

The doublets intensities must satisfy relation (4) which is also valid for the unsteady problem. Relation (4) is expressed on the middle of each side of the polygon. Up to now, no circulation around the profile, and then no jump of potential has been considered. Nevertheless, let us suppose that a jump of potential has been created at the trailing edge by a mean which will be defined later. The jump of potential must propagate, along the steady flow streamline originating from the trailing edge, with the local velocity $V_o(x,y)$. Both the streamline geometry and the velocity V_o have been determined by the computation of the steady case. The wake is then divided into n segments and prolonged downstream up to infinity by a straight line. The velocity n is supposed to be constant on each segment and equal to U_∞ on the straight line. A distribution of doublets is placed on the segment and on the straight line, their intensities obey to the condition of propagation with velocity V_o.

The induced velocities may be expressed by an analytical formula making use of the Complex Exponential Integral $E_1(z) = \int_z^{+\infty} (e^{-t}/t)\, dt$. When the frequency decreases towards zero, the jump of potential is constant all along the wake, and the induced velocities are those created by a concentrated vortex located at the trailing edge. The difficulties already encountered for the introduction of a circulation in the steady

case are happening here. The concentrated vortex must be distributed all over the profile perimeter. In the present case, doublets are used instead of vorticies, it has already been shown (3.2 b) that the variation in doublets intensity may replace a distribution of vorticies. This suggests to place doublets on the profile perimeter with an intensity $\Gamma(\xi)$ following a cubic law (Fig. 4). The variation of the intensity $\frac{d\Gamma}{d\xi}$ is zero at the trailing edge on the upper surface and on the lower surface.

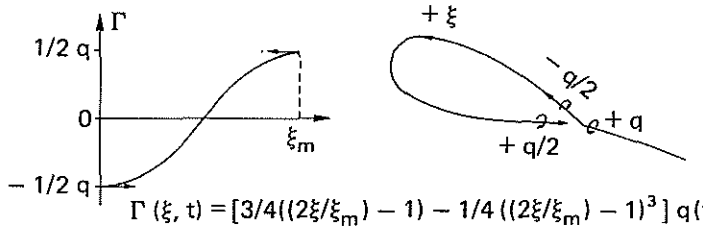

$$\Gamma(\xi, t) = [3/4((2\xi/\xi_m) - 1) - 1/4((2\xi/\xi_m) - 1)^3]\, q(t)$$

Fig. 4 — Doublets with intensity Γ (ξ, t) are placed on the profile perimeter to counter-balance the wake effect and to introduce a circulation around the profile.

At the trailing edge, the values of Γ are :

$\Gamma(0) = -\frac{q(t)}{2}$ on the upper surface

$\Gamma(\xi_{max}) = +\frac{q(t)}{2}$ on the lower surface.

The function $\Gamma(\xi)$ may be chosen arbitrarily, the only condition on it being to make compensation for the wake at the trailing edge. Thus, for simplicity, the phase of $\Gamma(\xi)$ has not been made to depend on the curvilinear abscissa ξ. The value of $q(t)$ must be determined by an additional equation. This equation is given by the unsteady Kutta-Joukowski condition expressed here as an equality of the unsteady pressures on the middle of the two segments close to the trailing edge.

d) Numerical results

In order to test the computer code, a comparison has been done with Theordorsen's theory. Unfortunately this theory is valid only for a flat plate in oscillation around a zero mean incidence and the present method becomes singular for a zero thickness profile. A first computation has been made for a NACA 0012 airfoil in oscillation around the fore quarter chord position. Derivative of the force $\frac{dF}{d\alpha}$ is plotted after normalisation against reduced frequency $k = \frac{\omega c}{2U_\infty}$; the real and imaginary parts are given in Fig. 5.

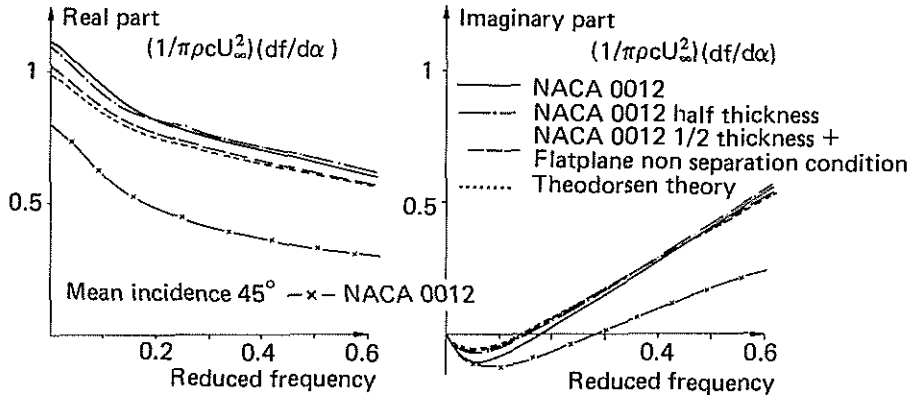

Fig. 5 — Real and imaginary parts of the lift coefficient on various profiles performing small pitch oscillations around a mean incidence of 0° and 45°.

At reduced frequency k = 0, the error on the real part is quite large : 11 %. A second calculation has been done for a profile deduced from the NACA 0012 by dividing its thickness by two. The numerical results for the now 6 % thickness profile shows some improvement specially for the imaginary part at low frequencies. On this 6 % profile, a third computation has been attempted for a better approximation of the flat plate. The unsteady non-separation condition has been replaced by the one relative to the flat plate, that is to say, the sources intensities calculated for the flat plate are imposed on the profile perimeter. This process improves further the results, specially for the real part of $\frac{dF}{d\alpha}$.

Of course the numerical method is not restricted to the case of a zero mean angle. For comparison, results are given for oscillations around an incidence α = 45°, with the assumption of a steady flow without separation. Though they are quite different from the Theodorsen's ; the shape of the curves remains unchanged.

5. Flow field around an obstacle with separation - Steady case

5.1. Study of the flow around a cylinder with a circular basis

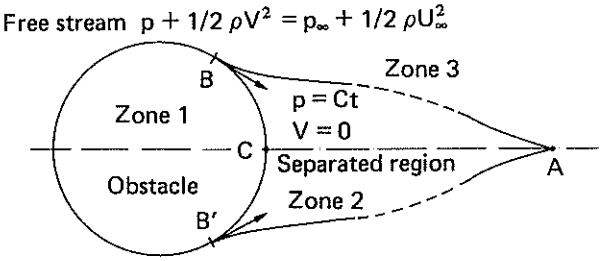

Fig. 6 – Description of a flow around a circular obstacle with separation by means of potential regions.

Following an idea proposed by Maskew and Dvorak in 1 , the separated region extending at the rear of an obstacle may be considered as a potential region (Fig. 6). The boundaries between the free stream region and the separated zone are in equilibrium, the normal component of the velocity is equal to zero. Thus, the separation region may be considered as a closed region where $\frac{d\varphi}{dn}$ = 0. In the case of an incompressible fluid, this involve a constant potential and a velocity equal to zero in the separated zone. If the velocity is zero, the pressure is constant, and thus it remains the same all along the free shear layers, boundaries between the separated region and the free stream. According to Bernouilli's law, velocity V in the free stream remains constant along the shear layers which appears as lines of vorticies with a constant intensity by unit length. Moreover, the layers are tangent to the obstacle at separations points B and B', at least as far as a perfect fluid is considered (no discontinuities in fluid velocity is allowed). In the same way, when the free shear layers intersect at point A, they have the same tangent, by symmetry in the direction of the fluid velocity at infinity. The obstacle, plus the separated region, can also been considered as a new profile, and point A is the trailing edge of this profile. A recompression must take place at the trailing edge ; this is not allowed here because the pressure must remain constant in the separated region. Point A must then be rejected at infinity downstream. Though such a model can be correct enough for some flows around a circular cylinder 9 , experiments show that the wake close quickly behind a profile due to the diffusion of the rotation in the free shear layers. Keeping in mind the extension towards flows

around a profile, the free shear layers are approximated in the computation by a set of linear segments and are interrupted at some distance downstream to the circle. The condition for the tangent at points B and B' has not been enforced, but vortex intensities by unit length $\pm \Gamma$ are imposed on the boundaries of the separated zone. The value of Γ is determined by an additional equation which makes the fluid total velocity to be zero at point C in the middle of the curvilinear segment BB'.

5.2. Flow field around a profile in the case of stall

The profile and the free shear layers are approximated by sets of linear segments. No boundary layer analysis has been attempted and the separation point D on the upper surface is chosen arbitrarily. The shear layer originating from D is made to be tangent to the profile. At the trailing edge, the shear layer bisects the acute angle of the profile, in order to minimise the problems of accuracy in the profile definition. The wake length is also chosen arbitrarily, but computations have shown an acceptable correlation with the experimental moment and drag curves only in the case of very short wakes. A constant vortex intensity by unit length $\pm \gamma_3$ exists on the free shear layers. To avoid large variations of induced velocities at separation point D and at the trailing edge, a distribution of vorticies γ_2 is placed on the profile out of the separated region. Intensity by unit length γ_2 varies according to a cubic law from the value $-\gamma_3$ at the separation point to the value $+\gamma_3$ at the trailing edge. The rate of variation of γ_2 is zero at both points. A circulation must also be introduced around the profile.

In much the same way as in the non-separated flow case (4.1.), another vortex distribution γ_1 is introduced on the profile, out of the separated zone, with a parabolic law.

5.3. Results obtained for the OA 209 profile

Experiments have been performed at the wind tunnel in Cannes. Lift, moments and drag coefficients have been measured (see Fig. 8, 9, 10). Because no boundary layer analysis has yet been included, no direct comparison can be made between theory and experiment. Nevertheless, some indirect correlations are still possible .

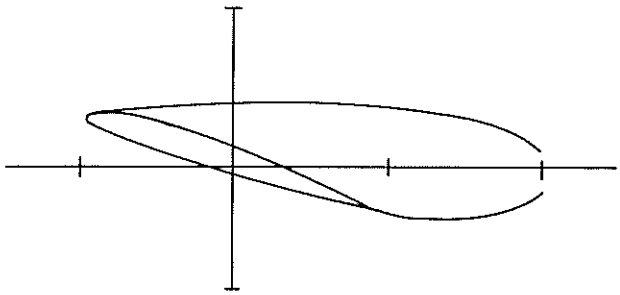

Fig. 7 – Example of computation for the OA 209 profile. Incidence 18°, separation point 96.49 %, wake length 0.5 chord. Sarting from two straight lines, the wake geometry is obtained in 9 steps. Computation time about 4 mn on a CYBER 750.

The separation point is imposed on the upper surface and the wake length is chosen. Early computations have been made with long wakes (5 chords), the results obtained for the moment and drag coefficients are out of

range. Reference 1 recommends very short wakes and it has been decided to choose a wake length of 0.5 chord. Because of the absence of boundary layer, it has not seemed useful to try an optimisation of the wake length. In all the presented results, the length remains the same at 0.5 chord (see Fig. 7). By varying the incidence and keeping the separation point at the same position, a lift curve is obtained. This curve is roughtly a straight line which intersects the experimental curve. Supposing that the theory is accurate enough, the point of intersection gives the incidence at which the separation point reachs its predefined position on the profile. By this process, the evolution of the separation point position on the profile upper surface may be obtained as a function of the incidence. A direct comparison for the separation point position is not possible with the available experiments on the OA 209, but the theory gives the pressure on the profile and then the moment and the drag. Thus, it is possible to obtain the moment and the drag for one incidence and its separation point position associated by means of the experimental lift curve. The moment and drag coefficients can then be compared (Fig. 9, 10) with the experimental ones. Though a much better correlation is possible by an optimisation of the wake length, the overall trends are well predicted, specially the large variations occuring after 15°. In the calculation of the drag, the introduction of skin friction would have still improved the results.

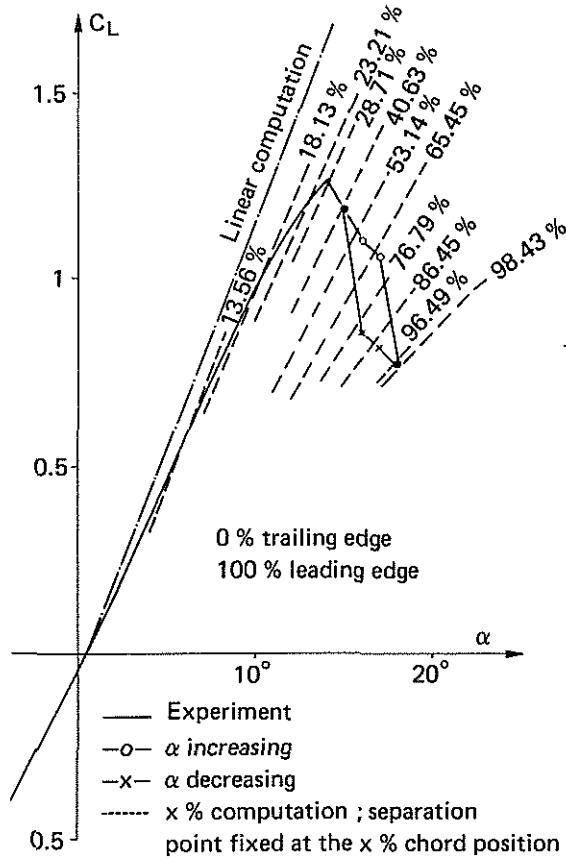

Fig. 8 – OA 209 profile, $U_\infty = 15$ m/s, chord 75 cm.

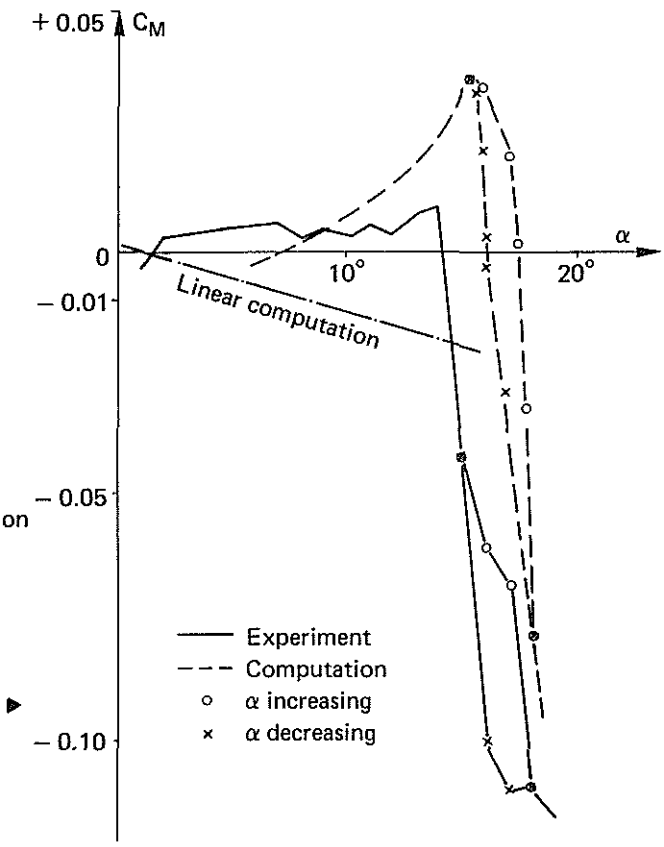

Fig. 9 – OA 209 profile, $U_\infty = 15$ m/s, chord 75 cm. Moment coefficient about the fore quarter chord position.

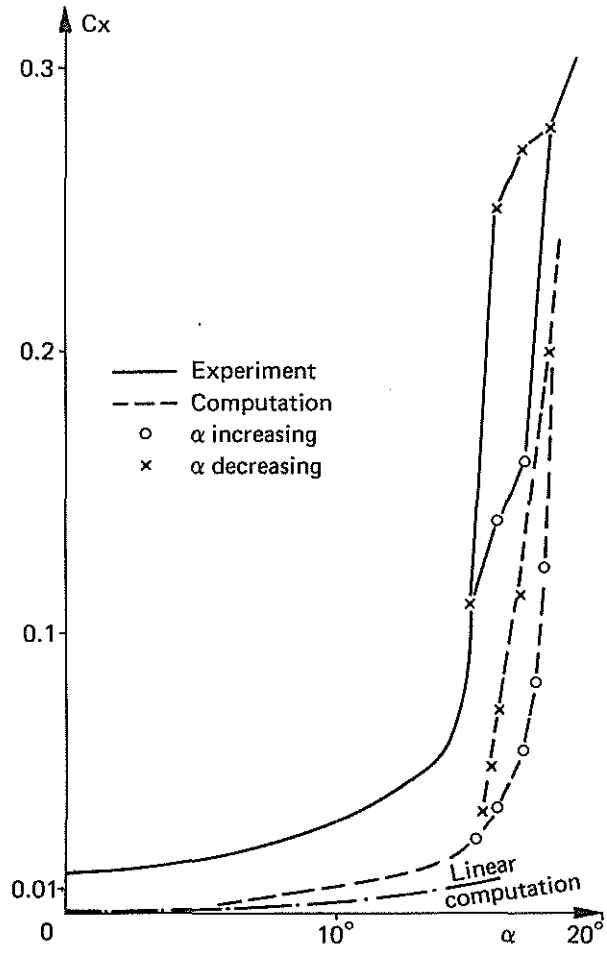

Fig. 10 – OA 209 profile, U_∞ = 15 m/s, chord 75 cm. Drag coefficient.

6. Flow field around an obstacle with separation - Unsteady case

The determination of the lift curve, of its maximum value, and of its evolution when stall is established, would have deserved a more complete study. Nevertheless, the unsteady stall is of prime importance in aeroelasticity, and much work has already been devoted to these questions at the ONERA's department of Structures 3, 4, 5 . The ONERA's semi-empirical model tries to achieve correct prediction of the lift and moment on a 2.D profile undergoing large amplitude oscillations. The input data in the ONERA's model are the steady curves and the unsteady forces generated on a profile by small oscillations around a mean given incidence. One of the aims of the present study is to furnish data for the ONERA's model. It is then necessary to extend the present theory towards unsteady computations. Only small oscillations are considered, and a solution is searched for by linearisation around a mean given steady flow.

6.1. Computation of the unsteady potential in the case of a separated flow

It has already been shown (4.2. a) that the potential φ is harmonic (relation 9). Green's formula (relation 3) can then be applied for the unsteady potential φ in each region where φ and its derivatives are continuous. By a combination of relation 3 written for each zone,

the potential φ in any region may be written as :

$$(19)\quad \varphi(P) = -\frac{1}{2\pi}\int_{profile}\left[K_1\frac{\partial\varphi}{\partial n} - \varphi K_2\right]ds - \frac{1}{2\pi}\int_{\text{Free shear layers}}\Delta\varphi K_2 ds - \frac{1}{2\pi}\int_{\text{unsteady rear wake}}\Delta\varphi K_2 ds$$

where $K_1 = \mathcal{L}og\, r$ is the source kernel

$K_2 = \frac{\partial}{\partial n}\mathcal{L}og\, r$ is the doublet kernel

$\Delta\varphi$ is the jump of potential across a boundary between two regions.

In oppositon to what happens in the steady case, the unsteady wake is believed to have an important extension even in the case of stall. It has been decided to introduce an unsteady wake beginning at the end of the separated zone and extending downstream up to infinity as in the unsteady case without stall (Fig. 11). Because of the finite, an even short, wake length considered in the steady case, there are some uncertainties on the origin of the unsteady wake as well as on its very existence in the case of movements with very low frequencies. In the present paper, the unsteady wake is a straight line, originating from the middle of the segment joining the extremities of the two free shear layers, and extending downstream to infinity. On the unsteady wake, the jump of potential must propagate with the local steady velocity V_0 as in 4.2. b. For simplicity the straight line is in direction of the undisturbed fluid velocity upstream and V_0 is equal to this velocity. A better treatment would be to replace the straight line by the actual streamline and to give to V_0 its local value.

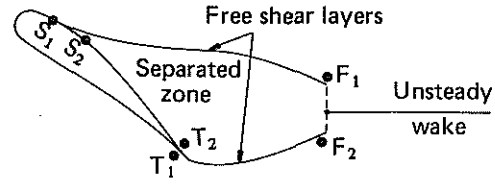

Fig. 11 – Physical scheme used in the case of unsteady computations.

6.2. Unsteady pressure in the case of a separated flow

Formula 15 is still valid in the case of a separated flow. Outside the separated region, the constant $p_0(t) = 0$, because the potentials and the pressure are all equal to zero at infinity. Inside the separated zone, $p_0(t)$ can be different from zero, and must be considered as one of the unknown coefficient of the problem.

6.3. Unsteady equations relative to the free shear layers

The free shear layers cannot support a jump in unsteady pressure. This fact provides a set of equations to determine the potential jump across the layers. If a sign + is affected to the potentials in the free stream, and a sign - to the potentials in the separated region, one obtains by means of 15 the following relation :

$$\rho\left\{\frac{\partial\varphi^+}{\partial t} + \varphi^+_{,\delta}\,\Phi^+_{,\delta}\right\} = \rho\left\{\frac{\partial\varphi^-}{\partial t} + \varphi^-_{,\delta}\,\Phi^-_{,\delta}\right\} + p_0(t)$$

This relation is valid on a set of non moving axes. It may be rewritten on a set of axes translating with the profile (as in 16). Neglecting the fluid velocity in the separated zone and taking it as V_o in the free stream, one gets :

$$(20) \qquad \rho \left\{ \frac{\partial \tilde{\varphi}^+}{\partial t} - \frac{\partial \tilde{\varphi}^-}{\partial t} + \tilde{\varphi}^+_{1\delta} V_{o\delta} \right\} = p_o(t)$$

As in the steady case, the free shear layers are approximated by a set of linear segments, and formula 20, which has no simple interpretation, is expressed on the middle of each segment. It has already been shown (formula 19), that a repartition of doublets with the unknown intensity by unit length $Q(\xi)$, must be placed on the separated zone boundaries. In order to discretise the problem, a set of $Q(\xi_i)$, values of $Q(\xi)$ on the segments extremities, is retained as the unknown coefficient of the problem, and the doublets intensity is supposed to vary linearly on the segments. If a free shear layer is approximated by n segments, there are $n + 1$ values of $Q(\xi_i)$ and only n equations resulting from the expression of formula 20 on the middle of each segment.

6.4. Supplementary equations

The equations of the unsteady problem are the classical equations of the potential on the profile, and the equations of the pressure jump on the free shear layers. The unknown quantities are the values of the doublets intensity on the profile, plus the value of the doublets intensity at the extremities of the free shear layers semgents, plus the value of $p_o(t)$. Three equations are needed to close the problem. These equations must be provided by physical assumptions of the same kind as the Kutta-Joukowski's conditions for the steady case, or for the unsteady problem without separation. Here it has been decided to write three conditions of equality for the pressures, one for the point of separation, another for the trailing edge, and the last one for the extremities of the free shear layers. As previously, the pressures are computed on the middle of a segment. If S_1 and S_2 are the middle of the segments adjacent to the separation point, T_1 and T_2 for the segments adjacent to the trailing edge and F_1 and F_2 the middle of the free shear layers last segment, we have (Fig. 11) :

$$P_{S1} = P_{S2}$$
$$P_{T1} = P_{T2}$$
$$P_{F1} = P_{F2}$$

The problem is now completely determined, but some comments must still be done on the condition at the separation point.

6.5. Variation of the position of the separation point on the profile upper surface

It has been assumed that the solution of the unsteady problem may be obtained by means of a linearisation around a predetermined steady solution. Then, only small displacements of the separation point, proportional to the amplitude of the profile oscillation are allowed. Nevertheless, the variations of pressure induced by these small displacements cannot be neglected 8 . On the profile upper surface, the pressure at the curvilinear abscissa x is given by :

$$P(x,t) = P_o(x) + p(x,t)$$

where $P_o(x)$ is the steady part of the pressure and p is the unsteady part supposed to be infinitely small.
When the separation point is not moving (artificial separation or acute

leading edge), one can write for the points S_1 and S_2 at the curvilinear abscissas x_1 and x_2 :

(21) $$P_o(x_1) + p(x_1,t) = P_o(x_2) + p(x_2,t)$$

On each side of the separation point, the static pressures are equal and relation (21) becomes :

(22) $$p(x_1,t) = p(x_2,t)$$

There is equality for the unsteady pressures in the case of a fixed separation point.

Let us now suppose a moving separation point, we still consider the equality of the pressures in the separated zone and in the free flow region. The curvilinear abscissas of S_1 and S_2 are now given by :

$$x_1(t) = x_1 + \delta x(t)$$
$$x_2(t) = x_2 + \delta x(t)$$

Relation (21) now becomes :

(23) $$P_o\left(x_1(t)\right) + p\left(x_1(t),t\right) = P_o\left(x_2(t)\right) + p\left(x_2(t),t\right)$$

δx is supposed to be infinitely small. By linearisation to the first order 23 is simplified into :

(24) $$P_o(x_1) + \delta x(t)\left[\frac{dP_o}{dx}\right]_{x=x_1} + p(x_1,t) = P_o(x_2) + \delta x(t)\left[\frac{dP_o}{dx}\right]_{x=x_2} + p(x_2,t)$$

Assuming that S_1 and S_2 are points close to the separation point but still fully on the free stream or on the separated region the derivatives $\frac{dP_o}{dx}$ may be defined. Moreover, we have $P_o(x_1) = P_o(x_2)$ and $\left[\frac{dP_o}{dx}\right]_{x=x_2} \simeq 0$. With these assumptions relation 24 becomes :

(25) $$p(x_1,t) + \delta x(t)\left[\frac{dP_o}{dx}\right]_{x=x_1} = p(x_2,t)$$

By using the pressure coefficient $C_p = \frac{P(x_1) - P_\infty}{\frac{1}{2}\rho U_\infty^2}$, formula (25) may be rewritten as :

(26) $$p(x_1,t) + \delta x(t)\left[\frac{1}{2}\rho U_\infty^2\right]\left[\frac{dC_p}{dx}\right]_{x=x_1} = p(x_2,t)$$

Relation (26) differs from (22) by the adjunction of a corrective term which necessitates the knowledge of $\delta x(t)$. In the case of small variations of incidence we have :

$$\delta x(t) = \frac{\delta x}{d\alpha}\, d\alpha(t)$$

The displacement of the separation point under the influence of a variation of incidence is known only for a vanishing frequency that is to say in the steady case. For the unsteady case, both the amplitude and the phase of $\frac{\delta x}{d\alpha}$ should be determined by a boundary layer analysis. The determination of $\frac{\delta x}{d\alpha}$ as function of the frequency has not been done so far. The computations will be presented with different values of the complex number $\frac{\delta x}{d\alpha}$.

6.6. Comparison between the theory and the experiment

Unsteady experiments have been recently realised at the CEAT wind tunnel in Toulouse 6, 7 . An OA 209 profile was oscillating with an

amplitude of $\pm$ 1° at various reduced frequencies $k = \frac{\omega c}{2U_\infty}$ ($0.05 \leq k \leq 1.274$). The mean value and the first harmonic of the forces have been recorded. No experiment has been realised in the steady case. On figure 12, the mean value of the lift coefficient is given. Unfortunately these mean values are dependent on the frequency and in spite of some scattering, the lowest value is almost always obtained for the lowest frequency. This suggests some non linear effect. It would be interesting to have other experiments done with less amplitude for the oscillations.

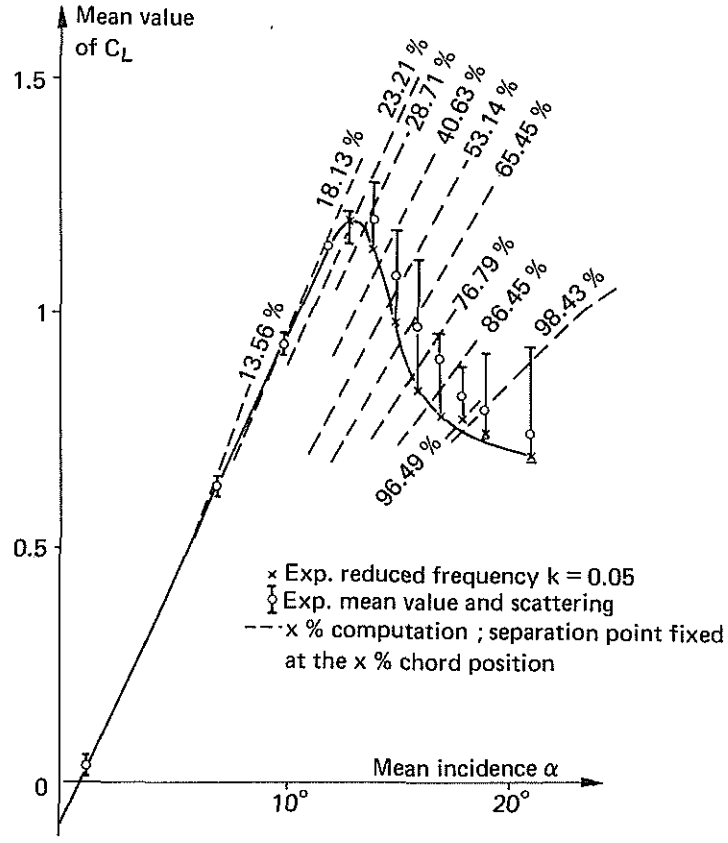

Fig. 12 – Mean value of the lift coefficient when the OA 209 profile is oscillating with an amplitude of ± 1° at various frequencies. Mach number 0.12, chord = 40 cm.

Here the curve obtained for the reduced frequency $k = 0.05$ has been taken as the steady curve, and the position of the separation point as function of the incidence is determined with the same process already used in the steady case (Fig. 8). It must be pointed out that the theoretical results do not give an explanation of the C_L value at large incidence. This may be due to the lack of boundary layer or to a bad choice of wake length. The displacement of the separation point is determined by the intersection of the experimental C_L curve with the set of lines resulting from the theory. This displacement is valid only for very low reduced frequencies, at higher frequencies the amplitude of the displacement may be thought to decrease and a delay to appear. To test for these hypothesis, three computations have been done :

$$-1)\quad \frac{\delta x}{d\alpha}(\omega) = 0$$

$$-2)\quad \frac{\delta x}{d\alpha}(\omega) = \frac{\delta x}{d\alpha}(\omega = 0)$$

$$-3)\quad \frac{\delta x}{d\alpha}(\omega) = e^{-j\frac{2\pi}{3}} \frac{\delta x}{d\alpha}(\omega = 0)$$

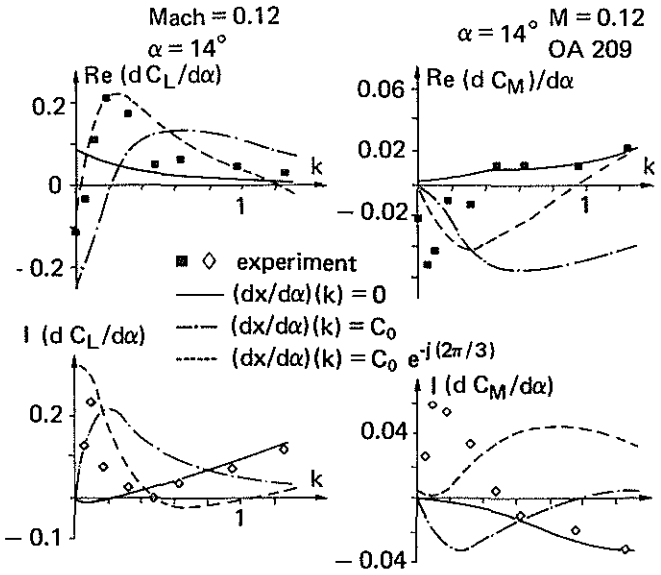

Fig. 13 — Real and imaginary parts of $dC_z/d\alpha$ and $dC_M/d\alpha$. Mean incidence 14° ; oscillations ± 1°; $k = \omega c/2U_\infty$ (reduced frequency). OA 209 profile Mach = 0.12.

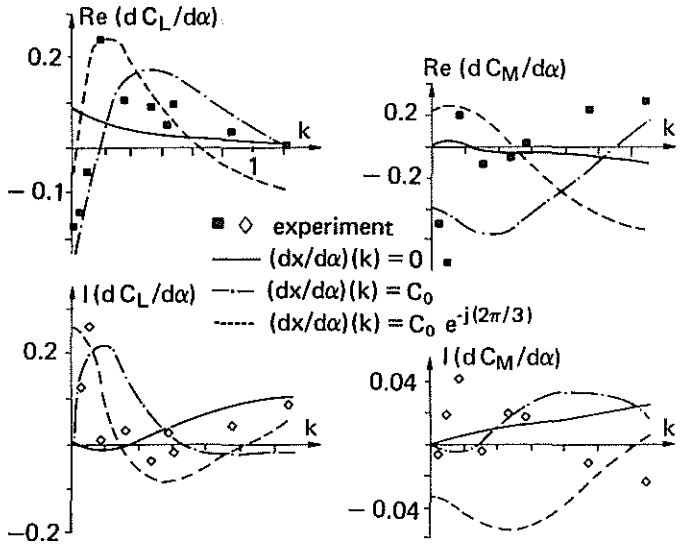

Fig. 14 — Real and imaginary part of $dC_z/d\alpha$ and $dC_M/d\alpha$. Mean incidence 15° ; oscillations ± 1°. Reduced frequency $k = \omega c/2$ V. OA 209 profile Mach = 0.12.

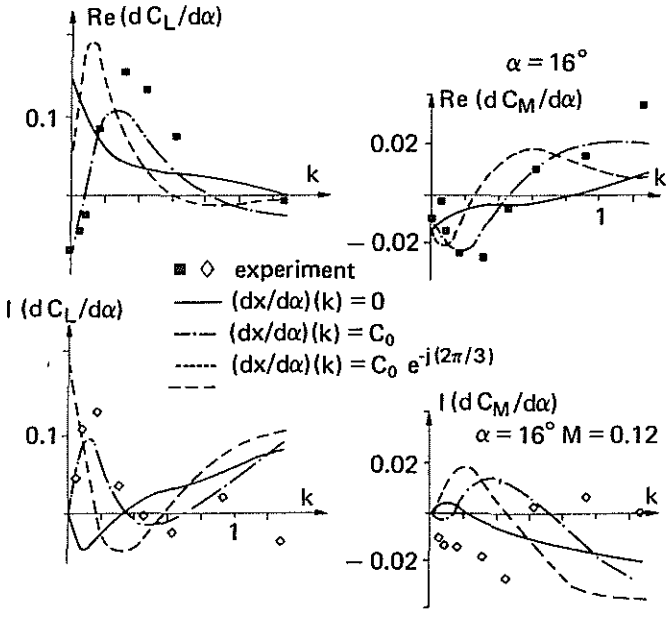

Fig. 15 — Real and imaginary part of $dC_z/d\alpha$ and $dC_M/d\alpha$. Mean incidence 16° ; oscillations ± 1°. Reduced frequency $k = \omega c/2\ V_\infty$. OA 209 profile Mach = 0.12.

The results are given on figures 13, 14, 15 for mean incidences α = 14°, 15°, 16°, and they may be compared with the experiment.
Let us examine the real and imaginary parts of $\frac{dC_L}{d\alpha}$, the variation of the lift coefficient with the incidence. With the first hypothesis, there is no displacement of the separation point and the theory gives results which look much the same as those on figure 5, obtained without separation. At low frequencies, there is no agreement with the experiment, but at frequencies higher than 1, the agreement is much better. Both hypothesis 2 and 3 give curves of the same trend, but it seems that a better agreement may be obtained with a large phase shift, even in the case of very low reduced frequencies. Though no direct comparison can be made with the experiment, the results are encouraging, and it seems that the theory has the possibility to explain the experimental results.

A comparison has also been attempted with the moment coefficient but a far greater precision is needed for this coefficient. Even the experiment does not show any definite trend for the imaginary part of $\frac{dC_M}{d\alpha}$. The next step, to improve the theory, should be the introduction of a steady boundary layer, and the adjustement of the wake length for a good agreement of the theory with both the C_L and C_M steady curves. With these new data, one can hope better results. One can also question the existence of a long unsteady wake, as well as the validity of relation 26, which can be an over simplification of the physical phenomenon at the separation point.

7. Conclusion

The development of a simplified theory has been undertaken for the prediction of the steady and unsteady forces on a profile in the case of a separated flow. Though the boundary layer has not been introduced so far, which precludes any direct comparison between the theory and the experiment, some qualitative results have already been obtained. For the unsteady case, the importance of the displacement of the separation point has been brought to light. With the introduction of a good unsteady condition for the separation point, one can hope to obtain satisfactory results, at least as far as the lift coefficient is concerned.

References

1) B. Maskew and F.A. Dvorak, The prediction of C_{Lmax} using a separated flow model. Journal of the American Helicopter Society, vol. 23 no 2, April 1978

2) Rao - Maskew. Flows over wings with leading edge vortex separation, NASA CR 165858 (1982)

3) D. Pétot, Progress in the semi-empirical prediction of the aerodynamic forces due to large amplitude oscillations of an airfoil in attached or separated flow, 9th European Rotorcraft Forum Stresa 13-15 sept. 1983, ONERA TP 1983-111

4) C.T. Tran, D. Pétot, Semi-empirical model for the dynamic stall of airfoils in view of the application to the calculation of responses of a helicopter blade in forward flight. 6th European Rotorcraft Forum Bristol Sept. 80, TP ONERA 1980-103

5) R. Dat, C.T. TRAN, D. Pétot, Modèle phénoménologique de décrochage dynamique sur profil de pale d'hélicoptère, XVIIIe Colloque d'aérodynamique appliquée (AAAF), Lille, Novembre 1979, TP ONERA 1979-149

6) J. Coulomb, Moyen d'essais pour l'étude de l'écoulement instationnaire autour de profils en oscillations harmoniques, XIVe Colloque d'aérodynamique applique (AAAF), Toulouse 1977

7) J. Coulomb, Profil OA2-09 essais instationnaires en oscillations harmoniques $\alpha = \pm 1°$, CEAT PV 104/SC

8) P.V.K. Perumal, F. Sisto, Lift and moment prediction for an oscillationg airfoil with a moving separation point, ASME paper no 74 GT 28 Oct., 1974

9) E. Szechenyi, Simulation de nombres de Reynolds élevés sur un cylindre en soufflerie, ONERA TP 1974-3, p. 155-164